Combustion and Flame 213 (2020) 26–38

Contents lists available at ScienceDirect

Combustion and Flame

journal homepage: www.elsevier.com/locate/combustflame

# Non-intrusive uncertainty quantification in the simulation of turbulent spray combustion using Polynomial Chaos Expansion: A case study

Benedict Enderle[a,*], Bastian Rauch[a], Felix Grimm[a], Georg Eckel[a], Manfred Aigner[a]

*German Aerospace Center (DLR), Pfaffenwaldring 38–40, Stuttgart 70569, Germany*

ARTICLE INFO

*Article history:*
Received 19 July 2019
Revised 12 November 2019
Accepted 13 November 2019

*Keywords:*
Uncertainty quantification
Sensitivity analysis
Polynomial Chaos Expansion
Spray combustion
Finite-rate chemistry

ABSTRACT

A major source of input uncertainties in the simulation of turbulent spray combustion is introduced by the need to specify the state of the liquid spray after primary breakup, i.e. a spray boundary condition for the lagrangian transport equations. To further enhance the credibility and predictive capabilities of such simulations, output uncertainties should be reported in addition to the quantities of interest. Therefore, this paper presents results from a comprehensive quantification of uncertainties from the specification of a spray boundary condition and numerical approximation errors. A well characterized lab-scale spray flame is studied by means of an Euler-Lagrange simulation framework using detailed finite rate chemistry. As direct Monte Carlo sampling of the simulation model is prohibitive, non-intrusive Polynomial Chaos expansion (PCE) is used for forward propagation of the uncertainties. Uncertain input parameters are prioritized in a screening study, which allows for a reduction of the parameter space. The computation of probabilistic bounds reveals an extensive uncertainty region around the deterministic reference simulation. In an a posteriori sensitivity analysis, the majority of this variance is traced back to the uncertain spray cone angle of the atomizer. The explicit computation of input uncertainties finally allows for an evaluation of total predictive uncertainty in the case considered.



## 1. Introduction

With the ever increasing availability of high performance computing capacities, high fidelity numerical combustion simulation is emerging as a powerful tool for the design, analysis and optimization of gas turbine combustors and associated combustion processes. This trend is motivated by the need for a reduction in tournaround time and cost in the design process as well as a detailed understanding of physical mechanisms in order to reduce pollutant emissions. Therefore, enormous progress has been made in numerical modeling of reacting flows [1–3]. Nonetheless, numerical modeling of turbulent spray combustion still involves major challenges stemming from the wide range of the characteristic scales of droplet dynamics, evaporation and mixing processes as well as two-phase interaction [4]. Rigorous model validation against experimental data represents a key feature to tackle these problems. Among the various approaches guiding the validation process [5–7], uncertainty quantification (UQ) methods have the potential to help understand sensitivities of simulation results to modeling uncertainties and therefore improve the models towards better physical representation [2].

Moreover, the various models involved require input quantities such as boundary conditions for the liquid phase which might be uncertain as they are difficult to measure in accompanying experiments. In an industrial design process, some of these quantities may be even unknown *a priori*, as they depend on the final design. In such cases, accurate quantification of simulation uncertainties is crucial for simulation credibility. As liquid fuel combustion will retain its importance for the aviation industry due to the high volumetric and mass energy density of liquid fuels, uncertainty quantification for spray combustion simulation is required to enable risk informed decision making in the design process of new combustor concepts.

In the general framework of UQ, uncertainties are classified as either aleatoric or epistemic. While the first describes an inherent variation in a quantity that could be characterized by a probability density function (PDF), the latter refers to uncertainties due to lack of knowledge [6]. The key part of a UQ analysis is then the propagation of the uncertainties through the simulation model. This requires transitioning from single computations to sampling based non-deterministic or probabilistic approaches. Due to the high computational costs in spray combustion simulation, the

* Corresponding author.
*E-mail address:* benedict.enderle@dlr.de (B. Enderle).

https://doi.org/10.1016/j.combustflame.2019.11.021

direct use of the high fidelity simulation as the forward model for inference purposes is excluded. Thus, efficient techniques to propagate uncertainty of a large number of parameters through simulation tools become necessary. While sensitivity analysis can help reduce the stochastic dimension of the problem and overcome the curse of dimensionality, surrogate models or stochastic expansions replacing the high fidelity simulation model are able to drastically reduce computation time in uncertainty propagation. From the class of stochastic expansion methods, Polynomial Chaos Expansion (PCE) [8] has drawn increasing attention for the use in UQ [9–11]. This method relies on a functional representation of random variables as an expansion in terms of orthogonal basis functions and is built on an efficient sparse sampling of the uncertain parameter space.

Although the future need for UQ in combustion simulations is recognized in the scientific community [2,3], only a few studies regarding its application can be found in the literature: The role of sensitivity and uncertainty analysis in combustion model validation was highlighted in the work of Mueller et al. [12] and Johnson et al. [13]. UQ was utilized in the analysis of sub-phenomena of combustion including acoustics [14], chemical kinetics [11], fuel evaporation [15] and spray boundary conditions [16]. The influence of uncertainties in chemical kinetics on a flamelet based Large Eddy Simulation (LES) of a methane jet flame was analyzed through stochastic collocation by Mueller et al. [17]. Pei et al. [18] conducted global sensitivity analysis for a URANS model of the Engine Combustion Network Spray A case to deduce the influence of spray parameters on integral quantities such as ignition delay and flame lift off height. Mueller et al. [19] and Tang et al. [20] combined PCE and LES of single phase flow to quantify the influence of boundary conditions on soot evolution and forced ignition, respectively. PCE based UQ was applied to an LES of a turbulent methane/hydrogen bluff-body flame by Khalil et al. [21] focusing on LES modeling parameters, e.g. Smagorinsky constant $C_s$. 1D marginal PDFs of mean axial velocity and temperature at a position in the flame were presented, showcasing the computational efficiency of PCE based UQ. Results from PCE based UQ were also reported by Masquelet et al. [22] for an industrial scale aviation gas turbine combustor. For the construction of the PCE, they conducted a series of flamelet based LES, assuming fast evaporation of the fuel and therefore neglecting the multiphase spray regime.

However, to the authors' knowledge, no study is available aiming on comprehensive uncertainty quantification of spray combustion simulation including detailed modeling of the combustion and multiphase regime, with a distinct focus on the specification of spray boundary conditions. As gas phase temperature distribution is closely connected to thermal loads, acoustic instabilities and the formation of pollutants, special emphasis should be put on the assessment of simulation credibility for this Quantity of Interest (QoI). Moreover, gas phase temperature is known to be highly sensitive to the prescribed condition of the fuel spray after atomization [23,24].

We therefore present a case study for the PCE based quantification of uncertainties arising from the specification of spray boundary conditions and numerical approximation errors of a RANS model. The proposed workflow consists of (a) analysis of input uncertainties in the simulation model, (b) assessment of the numerical error, (c) a screening study based on sensitivity analysis to reduce the stochastic dimension, (d) estimation of the PCE quality, (e) forward propagation of the input uncertainties through PCE, (f) determination of total output uncertainty. The predictive capability of the simulation model under the given uncertainties is appraised using experimental data.

The paper is structured as follows. A brief summary of the simulation framework is given in section 2 followed by the methods used for uncertainty quantification in section 3. The target flame for the case study is introduced in section 4 including a definition of the considered UQ problem. Thereafter, results of the proposed UQ workflow are presented and discussed (section 5). Finally, concluding remarks on the main findings are drawn in section 6.

## 2. Computational platform

A coupled Euler-Lagrange simulation framework consisting of separate solvers for the gaseous and dispersed spray phase is utilized for the acquisition of RANS data.

### 2.1. Gas field solver

The gaseous phase is calculated by the pressure-based DLR in-house code THETA (Turbulent Heat Release Extension of the TAU Code) [25,26] solving the incompressible, steady-state Reynolds Averaged Navier Stokes (RANS) equations including source terms for chemical reactions. THETA is a 3D finite volume solver for structured and unstructured dual grids. The effect of turbulence on the averaged quantities is modeled by the standard $k-\varepsilon$ turbulence model with canonical closure coefficients [27]. The convective and diffusive fluxes are discretized using second-order accurate quadratic upwind differencing schemes. The SIMPLE algorithm is applied to couple velocity and pressure.

### 2.2. Combustion modeling

In order to close the chemical source term in the RANS equations, reactions of gaseous species are modeled by a Finite-Rate Chemistry combustion (FRC) model where a separate transport equation is solved for each reactive scalar $\alpha$ [28]. The chemical source term from the FRC model is given by

$$\langle \omega_\alpha \rangle = M_\alpha \sum_{r=1}^{N_r} \left(\nu''_{\alpha,r} - \nu'_{\alpha,r}\right) \left[ \left\langle k_{f,r} \right\rangle \prod_{\beta=1}^{N_{sp}} C_\beta^{\nu'_{\beta,r}} - \langle k_{b,r} \rangle \prod_{\beta=1}^{N_{sp}} C_\beta^{\nu''_{\beta,r}} \right]. \quad (1)$$

$M_\alpha$ is the molar mass of species $\alpha$, $N_r$ the number of reactions and $\nu$ are the stoichiometric coefficients. Terms in square brackets denote sources of reactions which are controlled by the forward and backward rate coefficients $\langle k_f \rangle$ and $\langle k_b \rangle$. Modified Arrhenius equations

$$\langle k_r \rangle = A_r \left\langle T^{b_r} \right\rangle \exp\left(\frac{E_{a,r}}{R\langle T \rangle}\right) \quad (2)$$

are used for the calculation of averaged reaction rate coefficients based on the pre-exponential constant $A_r$, the temperature exponent $b_r$ and the activation energy $E_{a,r}$ of the reaction $r$. In the present study, a detailed chemical reaction mechanism for ethanol accounting for 38 species and 228 reactions is used [29].

Fluctuations in temperature and species due to turbulence are not resolved in the RANS context. Therefore, a turbulence-chemistry interaction model based on an assumed probability density function (aPDF) approach is included [28]. Two additional transport equations are solved: one for the temperature variance and one for the sum of the species' mass fraction variances. It is assumed that the temperature fluctuation follows a clipped Gaussian pdf while the species' mass fractions fluctuations follow a multivariate $\beta$-pdf [25]. Fluctuations are then included in the source term calculation in Eq. 1.

### 2.3. Dispersed phase modeling

The dispersed phase is computed using the DLR in-house simulation code SPRAYSIM [30] which is based on a Lagrangian particle tracking approach. Therefore, subsets of physical fuel droplets with

equal properties are replaced by numerical particles and simplified with a point source approximation. In this simplification particles are assumed to be discrete points providing point sources and point forces to the gas field [31]. Lagrangian particle tracking requires solving the coupled ordinary differential equations for particle position $\vec{x_p}$, particle velocity $\vec{u_p}$, particle diameter $d_p$ and temperature $T_p$ along the trajectory of each particle within the gas field. The ODEs are solved in SPRAYSIM by a predictor-corrector scheme with automatic step control. For a phase coupling, sources for momentum, energy and species are exchanged at runtime between THETA and SPRAYSIM via an iterative two-way-coupling procedure. Evaporation of droplets is modeled using the vaporization model of Abramzon and Sirignano [32], secondary breakup of droplets is accounted for through the Cascade Atomization and Breakup (CAB) model [33]. Unresolved turbulent dispersion of droplets is included by a variant of the Gosman-Ioannides model [34]. Further details on modeling and implementation in SPRAYSIM are given in [35] and [36].

## 3. Non-Deterministic (probabilistic) approach for uncertainty quantification

From a theoretical point of view, sources of uncertainties of a given simulation model can be subdivided into three major categories, namely numerical uncertainties, model form and input uncertainties [6]. Numerical uncertainties take errors into account arising from the approximation of the differential equation based model, such as discretization error, iterative convergence error or round-off errors. Model form uncertainties stem from the process of abstraction and formulation of the mathematical models and can be categorized into omission, aggregation and substitution types [6]. Finally, input uncertainties include parameters used in the simulation model or its sub-models as well as data describing the surrounding of the system, e.g. boundary conditions.

The present study is focused on input uncertainties and numerical uncertainties. While the latter is addressed by a rigorous error analysis and extrapolation of the RANS model, input or parametric uncertainties have to be propagated through the simulation model $\mathcal{M}$ to determine variability and therefore uncertainties in the observed quantities $Q$. We employ a non-intrusive strategy where $\mathcal{M}$ is treated as a black-box problem and probabilistic behavior is inferred from a finite number of random evaluations of $\mathcal{M}$ [7].

The most straight-forward technique to draw these random evaluations is the well established Monte Carlo method [37]. The main drawback is that this procedure requires a relatively large number of system evaluations ($\mathcal{O}(10^3 - 10^4)$) to yield reliable statistics, making it prohibitive for large scale simulation problems. One way to overcome this limitation is to replace the high fidelity simulation model by a suitable statistical emulator or surrogate model $\mathcal{M}_{SM}$, taking into account minor approximation errors [38]. Statistical measures are then computed from sampling of the cheap-to-evaluate surrogate model or analytical relationships as in the case of Polynomial Chaos Expansion. A summary of the probabilistic methods used in the present study is given in the following.

### 3.1. Sensitivity analysis

Due to the high modeling demand in turbulent spray combustion simulations, a large number of inputs for $\mathcal{M}$ exist in the case considered resulting from modeling parameters as well as boundary conditions. Morris One At a Time (MOAT) sensitivity analysis is used to identify the most influential parameters in an *a priori* screening study. Based on these results, the input parameter space is reduced by fixing minor parameters to constant values [39]. Following the uncertainty quantification (*a posteriori*), Sobol' indices are calculated to assess the contribution of each parameter to the total uncertainty in the simulation.

#### 3.1.1. Morris One At a Time (MOAT)

In a MOAT analysis [40], input parameters $\xi_i$ are varied one at a time with a substantial variation step size $\Delta$ while the afore changed parameter remains at the changed value. An elementary effect associated to this variation is computed through the forward difference

$$d_i = \frac{Q\left(\boldsymbol{\xi} + \Delta e_i\right) - Q\left(\boldsymbol{\xi}\right)}{\Delta}, \tag{3}$$

where $e_i$ is the coordinate vector of the changed parameter in the respective variable subspace. The distribution of elementary effects $d_i$ over the input parameter space represents the effect of input $\xi_i$ on the output $Q$. After generating $r$ samples, mean $\mu_i$ and standard deviation $\sigma_i$ of the elementary effect $d_i$ are approximated by

$$\mu_i = \frac{1}{r}\sum_{j=1}^{r} d_i^{(j)} \quad \text{and} \quad \sigma_i = \sqrt{\frac{1}{r}\sum_{j=1}^{r}\left(d_i^{(j)} - \mu_i\right)^2}. \tag{4}$$

The mean gives an indication of the overall effect of an input on the output, standard deviation implies nonlinear effects or interactions between parameters. Thus, $\xi_i$ can be ranked by $\mu_i$ and $\sigma_i$.

#### 3.1.2. Sobol' indices

Variance-based sensitivity methods such as Sobol' indices [41] offer a more detailed insight into the sensitivity structure of a given quantity of interest. This method is based on the decomposition of the total variance $\mathbb{V}$ of a model output $\mathcal{M}(\boldsymbol{\xi})$ into contributions from the different inputs $\mathbb{V}[\mathcal{M}(\boldsymbol{\xi})|\xi_i]$. We consider the first order indices $S_i$ which account for the direct contribution to the variance of $\mathcal{M}$ from $\xi_i$, and the total-effect index $S_i^T$ [42] which also includes interaction effects of $\xi_i$ with $\xi_{\neq i}$:

$$S_i = \frac{\mathbb{V}\left[\mathbb{E}\left[\mathcal{M}\left(\boldsymbol{\xi}\right)|\xi_i\right]\right]}{\mathbb{V}\left[\mathcal{M}\left(\boldsymbol{\xi}\right)\right]}, \quad S_i^T = \frac{\mathbb{V}\left[\mathcal{M}\left(\boldsymbol{\xi}\right)|\boldsymbol{\xi}_{\sim i}\right]}{\mathbb{V}\left[\mathcal{M}\left(\boldsymbol{\xi}\right)\right]}. \tag{5}$$

### 3.2. Uncertainty propagation - Polynomial Chaos Expansion

For the non-intrusive propagation of input uncertainties through the simulation model the method of Polynomial Chaos Expansion (PCE) is adopted [8,43,44]. Quantities of Interest $Q$ are interpreted as random variables driven by $n_s$ inputs from the uncertain input space $\Omega$. Within the framework of PCE, $Q$ can be represented as a spectral expansion in terms of orthogonal functions of a vector of standard random variables $\boldsymbol{\xi} = (\xi_1, ., \xi_{n_s}) \in \Omega$ having finite variance. The general PC expansion is given as

$$Q = f\left(\boldsymbol{\xi}\right) = \sum_{k=0}^{\infty} \alpha_k \Psi_k\left(\boldsymbol{\xi}\right), \tag{6}$$

where $\alpha_k$ are the expansion coefficients or modes and $\Psi_k$ are multivariate polynomials of $\boldsymbol{\xi}$. It is required that the polynomials $\Psi_k$ form a complete orthogonal basis with respect to the measure on $\boldsymbol{\xi}$. Taking advantage of this property an equation for the PCE coefficients can be derived as

$$\alpha_k = \frac{\left\langle f\left(\boldsymbol{\xi}\right)\Psi_k\right\rangle}{\left\langle \Psi_k^2\right\rangle}, \tag{7}$$

where

$$\left\langle f\left(\boldsymbol{\xi}\right)\Psi_k\right\rangle \equiv \int_{\Omega} \Psi_k \rho\left(\boldsymbol{\xi}\right) f\left(\boldsymbol{\xi}\right) \mathrm{d}\boldsymbol{\xi} \tag{8}$$

and $\rho$ is the density of $\boldsymbol{\xi}$ over $\Omega$ [44].

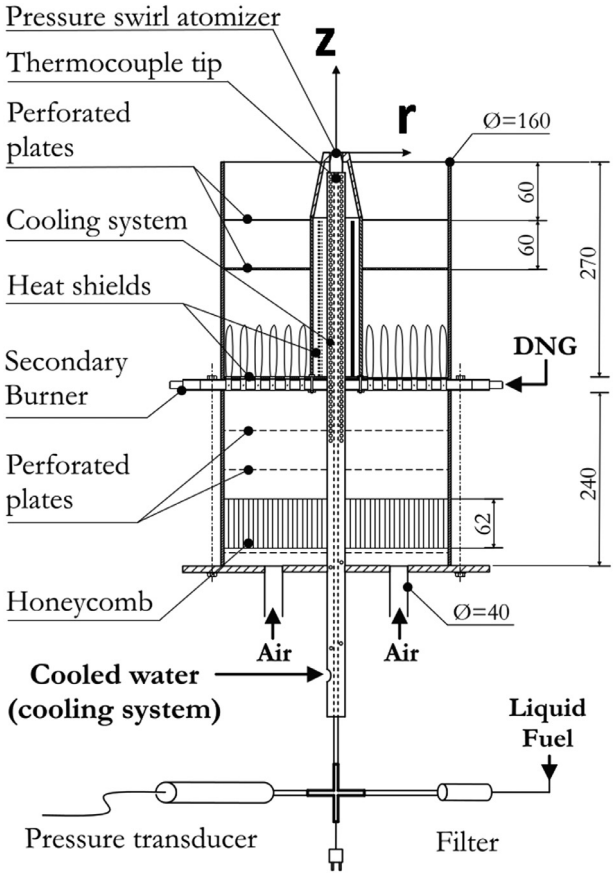


**Fig. 1.** Schematic of the DSHC burner [46].

However, for practical computations, the infinite series from Eq. (6) is usually truncated to a certain total degree of $p$ resulting in the approximation $\mathcal{M}_{PCE}$:

$$f(\boldsymbol{\xi}) \approx \sum_{k=0}^{P} \alpha_k \Psi_k(\boldsymbol{\xi}) = \mathcal{M}_{PCE} \tag{9}$$

with cardinality $P$ of

$$P+1 = \frac{(n_s+p)!}{n_s!\,p!}. \tag{10}$$

Note that for a given PCE the corresponding mean $\mathbb{E}$ and variance $\mathbb{V}$ can be computed directly from the PCE components as

$$\mathbb{E}[\mathcal{M}_{PCE}] = \alpha_0 \quad \text{and} \quad \mathbb{V}[\mathcal{M}_{PCE}] = \sum_{k=1}^{P} \alpha_k^2 \langle \Psi_k^2 \rangle. \tag{11}$$

Consequently, this allows to calculate the Sobol' indices as presented in Eq. (5) analytically as a post-processing step of the PCE coefficients without further sampling of the model [45].

## 4. Test case and UQ problem

The aforementioned methods are applied to the Delft Spray in Hot Coflow (DSHC) Flame [46] due to its simple geometry and available comprehensive experimental and numerical results. As depicted in Fig. 1, the burner consists of a cylindrical hot coflow generator fed by the lean combustion of Dutch Natural Gas (DNG) to increase the airflow temperature and dilute the air with combustion products prior to the primary combustion zone. A commercial hollow cone pressure swirl atomizer (Delavan WDA 0.5 GPH) is installed in the center of the coflow generator. The atomizer forms a fine spray of ethanol droplets which quickly evaporate and feed a stable lifted-off flame above the burner. For further reference, a coordinate system is shown in Fig. 1 with its origin placed at the atomizer orifice.

**Table 1**
Reported mean coflow properties.

| Case | $T_{cf}$ [K] | $U_{cf}$ [m s$^{-1}$] | $I_{cf}$ [%] |
|---|---|---|---|
| $\mathbf{H_{II}}$ | 1400 | 2.5 | 2.0 |

Radial profiles of gas phase temperature and droplet sizes over the reaction zone are available from Coherent Anti-Stokes Raman Scattering (CARS) and Phase Doppler Anemometry (PDA) measurements, respectively [46]. Measurement data was collected at different heights above the atomizer ($z = \{15,\ 20,\ 30,\ 40,\ 50,\ 60\}$ mm). In addition, gas phase velocity components, temperature and $O_2$ volume fraction were measured along the radial direction at the coflow exit ($z = 0$ mm) to characterize the coflow after the secondary combustion zone.

Different operating conditions of the burner were investigated in the experiments. However, this study focuses on one of the ethanol spray in hot-diluted coflow cases, namely case $\mathbf{H_{II}}$.

### 4.1. Computational domain and gas phase boundary conditions

In the computational domain, only the region above the atomizer is considered while the secondary DNG burner is not simulated explicitly. Properties of the coflow after secondary combustion are prescribed through a boundary condition based on the radial profiles of temperature and its fluctuations, velocity components, turbulence properties and gas phase composition from the experimental characterization. Resulting mean coflow properties are summarized in Table 1.

The computational domain is reduced to an axisymmetric 20° wedge, due to the statistical rotational symmetry of the flame. A region of 300 mm axial and 150 mm radial extent is considered. An ambient airstream with $U_{amb.} = 0.1\,\mathrm{m\,s^{-1}}$ surrounds the coflow inlet for numerical stability. Three different grids are considered in this study, all relying on the same fully structured, orthogonal grid topology. The reference grid consists of approximately $80 \cdot 10^3$ elements, while the coarse and the fine grid incorporate half and twice the number of elements, respectively. Grid refinement strategies proposed by Roache [5] where followed in order keep main characteristics of the grid consistent over the three levels of resolution. An overview of the grid cell spacing $\Delta$ along the axial and radial direction is given in Fig. 2. For brevity, only every $10^{th}$ gridpoint is shown. In the reference grid, cell spacing ranges from 0.5 mm in the liquid injection region ($R < 10$ mm) to 2 mm at the end of the computational domain. The stream-wise grid points follow a linear expansion law up to a maximum cell size with a growth factor of 1.01. Therefore, strong clustering is achieved in regions where droplet evaporation and flame stabilization occurs. Unless otherwise stated, all results in the following are computed on the reference grid.

### 4.2. Dispersed phase boundary conditions

To avoid the modeling and simulation of the complex phenomena such as liquid sheet breakup, ligament formation and droplet collision occurring in the dense spray region during primary atomization of the liquid fuel [31], a boundary condition for the droplets in the dilute spray region is specified. Hence, properties of the droplets after primary atomization have to be stated.

In the simulation, a 20° segment of an injection disk with diameter $d_{in} = 1$ mm at a distance of $z_{in} = 1$ mm from the actual

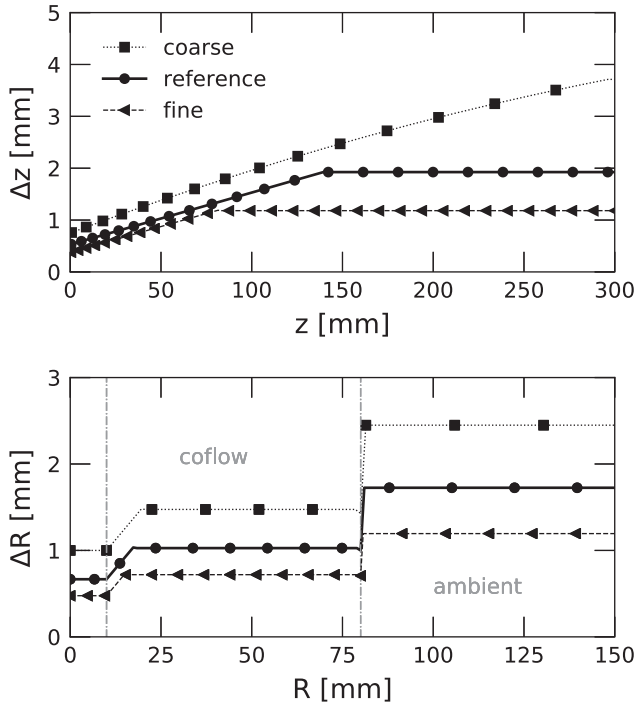


**Fig. 2.** Grid cell spacing along the axial ($\Delta z$) and radial direction ($\Delta R$) in the used structured grids.

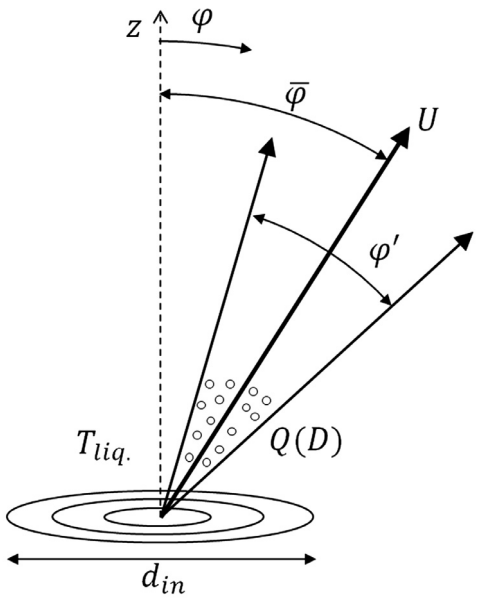


**Fig. 3.** Spray boundary condition and input parameters at the injection plane.

atomizer orifice defines the boundary condition of the liquid droplets. The distance $z_{in}$ resembles the mean liquid sheet breakup length of the pressure-swirl atomizer under the given conditions and is inferred from preliminary calculations with the LISA primary breakup model [47]. An illustration of the input parameters and geometric quantities at the injection disk is given in Fig. 3: A mean trajectory angle $\bar{\varphi}$ resembling the half opening angle of the hollow cone is augmented with a dispersion angle $\varphi'$ since the effect of flash boiling atomization as present in the $\mathbf{H_{II}}$ case [46] tends to increase the spray angle [48]. Furthermore, a constant absolute droplet starting velocity $U_D$ and a liquid droplet temperature $T_{liq}$ is set. The droplet size spectrum of the polydisperse spray is modeled by a Rosin-Rammler (RR) distribution,

**Table 2**
Nomenclature for parameters of the droplet boundary condition.

| | |
|---|---|
| $D_0$: | Mean droplet diameter in the RR distribution |
| $U_D$: | Starting velocity of fuel droplets |
| $\bar{\varphi}$: | Mean trajectory angle of droplets |
| $\varphi'$: | Trajectory dispersion angle |
| $T_{liq}$: | Starting temperature of fuel droplets |
| $q$: | Spread of the RR distribution |

$$Q(D) = 1 - \exp\,(D_0/D)^q \quad \text{with} \quad D_0 = \mathrm{SMD}\left[\Gamma\left(1 - \frac{1}{q}\right)\right] \tag{12}$$

and the size distribution factor $q$ representing the spread of the distribution.

For the steady state simulations, approximately $20 \cdot 10^3$ computational particles with varying trajectory angle $\varphi \in \left[\bar{\varphi} - 0.5\varphi'; \bar{\varphi} + 0.5\varphi'\right]$ are sampled from the size distribution. Thus, an overall liquid mass flow of $\dot{m}_{liq} = 0.081\,\mathrm{kg\,s^{-1}}$ is injected into the computational domain. A nomenclature of the parameters of the droplet boundary condition is given in Table 2.

### 4.3. Characterization of uncertain input space

Due to the fact that the gaseous phase boundary conditions are precisely defined by the experimental characterization of the coflow, the study on input uncertainties of the DSHC flame is focused on the dispersed phase boundary condition. In the spray boundary condition as defined in the previous section, six parameters remain to be determined. As the measurement of droplet data in the transition regime from dense to dilute spray is challenging and subject to large measurement errors [49], the first available data is at a distance of $z = 8\,\mathrm{mm}$ from the atomizer orifice. Furthermore, some reported characteristics of the atomizer are either incomplete ($\varphi'$), highly uncertain ($T_{liq}$) or potentially wrong ($U_{liq}$). For example, Ma et al. [50] pointed out that using the droplet injection velocity based on the experimental data of the atomizer, the downstream velocity will be significantly over predicted.

Consequently, parameters of the spray boundary condition have to be calibrated against the downstream experimental data resulting in a best fit for the used simulation methods and models. As a consequence, different values for these parameters are found in the literature on simulations of the DSHC flame. Although in each of the studies a slightly different scheme for the construction of the spray boundary condition was utilized, main parameters as defined previously can be identified and compared:

For a RANS simulation with a Flamelet Generated Manifold (FGM) combustion model, Ma et al. [51] computed the parameters with the LISA primary breakup model [47]. In a similar setup, Jamali [52] considered slightly different inputs for the LISA model. Gallot-Lavallée et al. [53] conducted an LES with a stochastic fields combustion model and derived a PDF for the injection angle as a function of the droplet diameter. In a further LES/FGM study, Ma et al. [50] proposed a conditional droplet injection model for the DSHC case. A calibrated spray boundary condition for the THETA/SPRAYSIM framework was presented using LES and FRC by the authors [24]. As an example for the variation of input parameters over the mentioned studies, Fig. 4 gives a comparison of the cumulative drop size distribution from different simulations of the DSHC $\mathbf{H_{II}}$ case.

For the present study, we consider the six input parameters of the spray boundary condition from Table 2 as uncertain. The uncertain input space is constructed from the respective minimum and maximum values found in the aforementioned literature as they all demonstrated good agreement with the experimental data of the test case. Since no further information is available, all six

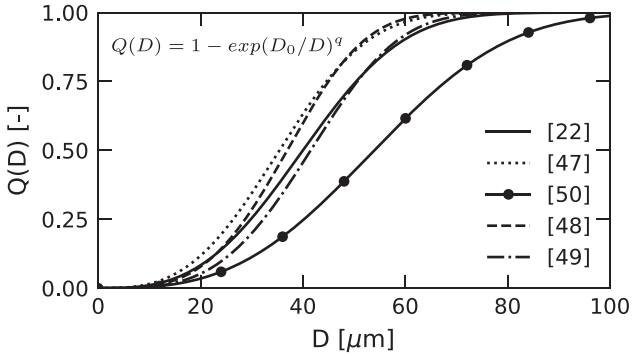


**Fig. 4.** Cumulative drop size distributions from different simulations of DSHC H-II.

**Table 3**
Minimum and maximum bounds of the epistemic uncertain inputs.

| | $D_0$ [$\mu$m] | $U_D$ [m s$^{-1}$] | $\bar{\varphi}$ [°] | $\varphi'$ [°] | $T_{liq}$ [K] | $q$ [−] |
|---|---|---|---|---|---|---|
| **Minimum** | 40 | 27.3 | 30 | 6 | 300 | 3.0 |
| **Maximum** | 45 | 35.7 | 40 | 20 | 310 | 3.5 |
| *Exp.* [46] | – | 51.7[a] | 30[b] | – | 301 | – |
| *LES* [24] | 42.5 | 35.7 | 30 | 20 | 301 | 3 |

[a] Liquid velocity at the atomizer exit ($U_{liq}$)
[b] Nominal value for Delavan WDA 0.5 GPH atomizer

input quantities are treated as purely epistemic interval-valued uncertainties, bounded by the respective minimum and maximum as summarized in Table 3. Note that $U_D$ from the experiment given in Table 3 is not the droplet starting velocity but the calculated velocity of the liquid fuel at the atomizer exit based on fuel mass flow rate, fuel density and injector exit diameter.

Since gas phase temperature data is one of the major output quantities of a spray combustion simulation, the radial temperature profiles at different heights above the atomizer are considered as QoIs for the following case study.

## 5. Results

A comparison of RANS simulation and LES results from a previous study [24] with the same simulation framework is given in Fig. 5. In both cases, the same parameters for the spray boundary condition as depicted in Table 3 were applied. In the following, we will denote these RANS results as the deterministic reference simulation. For brevity, only results at $z = 15$ mm and $z = 40$ mm are displayed. Due to the radial bias in the experimental data of temperature [46], especially in the region of strong gradients, experimental results for both $R < 0$ mm and $R > 0$ mm are included. Based on typical accuracy of CARS measurements [54,55] 5% error bars are imposed on the experimental data.

At both axial positions, three characteristic features of the flame are visible [56]:

(I) Gas phase temperature drops below the coflow temperature along the centerline due to strong evaporation of fuel droplets and therefore absorption of enthalpy from the gas-field
(II) An inner and outer flame front characterized by strong radial gradients in temperature
(III) Maximum temperature increase with respect to the inlet temperature stays below the self-ignition temperature of the mixture ($T_{si} = 706$ K)

As evident from Fig. 5, the RANS simulation is able to reproduce all of these characteristics. At $z = 40$ mm and further downstream, both simulations predict a higher flame spread leading to radial temperature deviations. This tendency was also reported

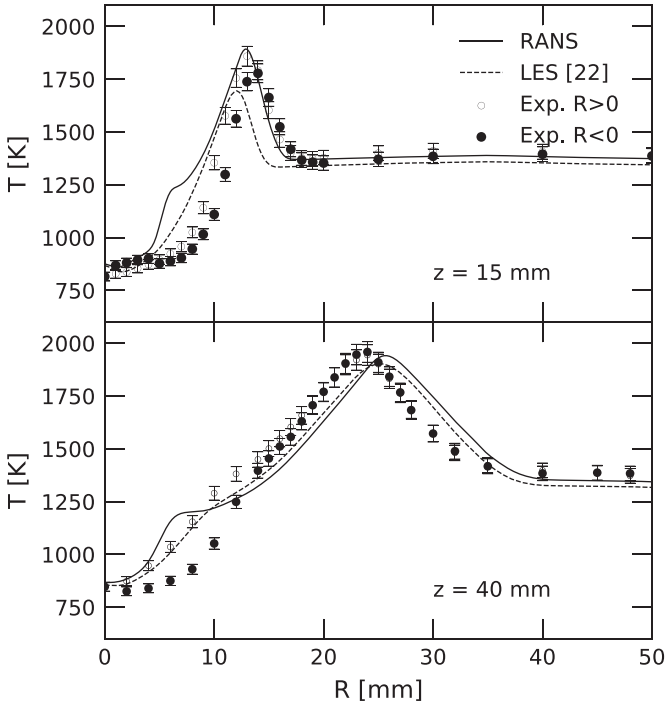


**Fig. 5.** Radial profiles of mean gas phase temperature at $z = 15$ mm and $z = 40$ mm from LES [24] and RANS.

by [53] and [57]. Note that the spread is larger in the RANS than in the LES. A major deviation of the RANS from both experiment and LES is found at the beginning of the inner averaged reaction zone ($R \approx 5$ mm). Considering that this deviation is present at all axial positions it is concluded that this must be a systematic error of the RANS. The absence of resolved unsteady flow structures in the RANS and their influence on particle dispersion, droplet evaporation and local fuel mixing could be a key factor causing these deviations. For example, Abani et al. [58] pointed out that RANS models are prone to errors in the near injector region, where phase-coupling effects play a significant role. Furthermore, one should keep in mind that the spatial grid resolution in this area for the LES is well above the RANS. In the next section, it is shown that this area is subject to considerable numerical uncertainties. Still, the RANS simulation provides a suitable accuracy for the following uncertainty study.

In terms of computational costs the RANS setup drastically reduces the required CPU hours by a factor of 70 for a single computation compared to the LES.

### 5.1. Numerical uncertainties

We use the reference RANS simulation from the previous section for a systematic evaluation of numerical uncertainties in the used simulation approach. Generally speaking, these uncertainties arise from discretization error, iterative convergence error, roundoff error and errors due to computer programming mistakes [7]. The latter two are assumed to be negligible due to previous and ongoing verification and validation efforts for our simulation framework. From the inspection of residuals and their convergence, iterative errors are expected to be in the order of machine accuracy. Therefore, special emphasis is put on discretization errors stemming from spatial grid resolution.

To evaluate this error, the grid convergence method proposed by Roache [5] is adopted. It relies on the analysis of multiple solutions from a sequence of grids with decreasing grid spacing $h$. For the case considered, a coarse ($f_3$) and fine ($f_1$) mesh with

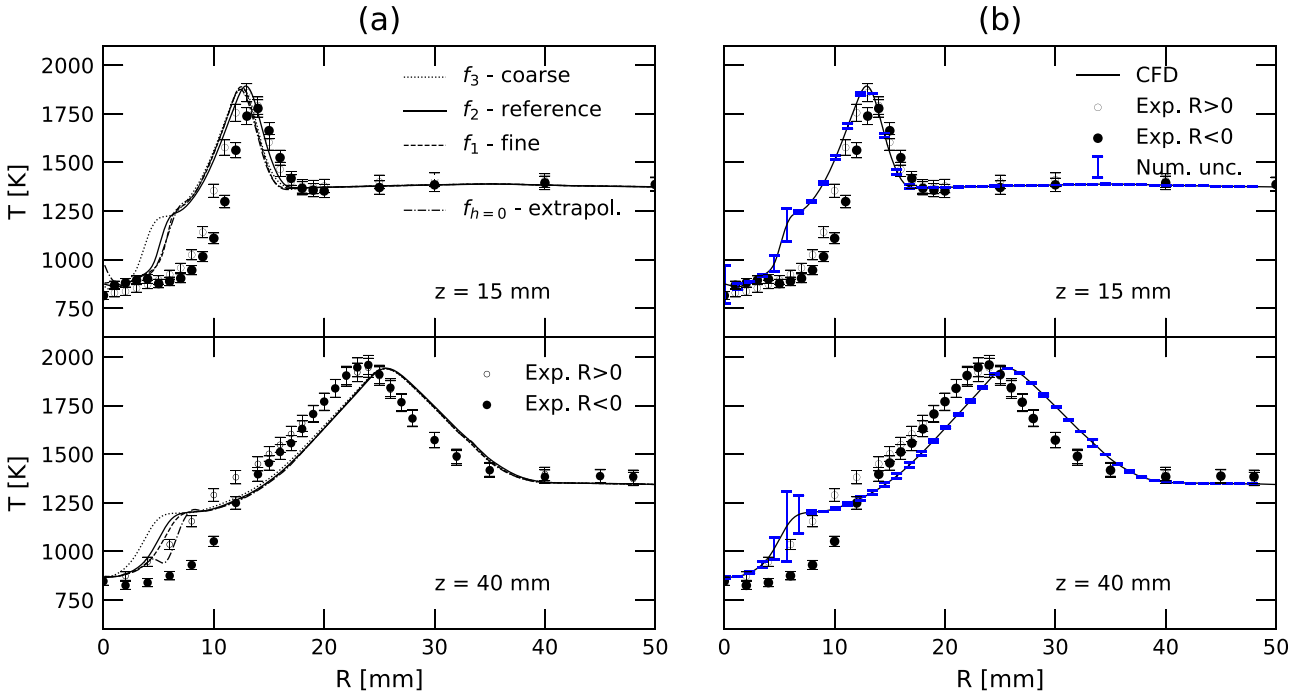


**Fig. 6.** Results from grid convergence study and associated numerical uncertainties.

respect to the reference ($f_2$) is used, keeping the refinement ratio $r = h_{i+1}/h_i$ constant at $r = \sqrt{2}$. The influence of grid resolution on the radial temperature profiles is displayed in Fig. 6 (a). Highest sensitivity is found at the beginning of the inner averaged reaction zone ($R \approx 5$ mm) at both axial positions. Apart from that, the solution is nearly insensitive to grid refinement at $z = 40$ mm. In order to get a quantitative assessment of sensitivity to grid resolution, the temperature profiles are extrapolated to a hypothetical infinitely small grid spacing $h = 0$ using Richardson extrapolation [5]. An observed order of convergence $p$ is calculated by

$$p \equiv \frac{\log\left(\frac{f_2 - f_1}{f_3 - f_2}\right)}{\log r}. \tag{13}$$

As Stern et al. [59] pointed out, this equation is not robust especially in cases where the datapoints $f_i$ are nearly constant with change in grid size or when $f_2 - f_1 < f_3 - f_2$. We therefore limit $p$ to an interval $[p_{min}, p_{max}]$ with $p_{min} = 0.5$ and $p_{max} = 3$ as recommended by [60]. The extrapolated solution is then determined by

$$f_{h=0} = f_1 + \frac{f_1 - f_2}{r^p - 1}. \tag{14}$$

A cubic interpolation is used to transfer the medium and fine grid solution to the coarse mesh locations. Extrapolated profiles are included in Fig. 6 (a). The numerical error $\varepsilon_{num} = |f_{h=0} - f_2|$ is low and the reference grid $f_2$ represents an appropriate spatial resolution of the problem. Based on $\varepsilon_{num}$, numerical uncertainties $U_{num}$ are estimated using the approach proposed by Roy and Oberkampf [7]:

$$U_{num} = F_s \varepsilon_{num} = F_s |f_{h=0} - f_2|, \tag{15}$$

with a safety factor $F_s$ which is recommended to be 1.25 for extrapolations involving three or more grids. Resulting uncertainties are included as error bars in the reference simulation results in Fig. 6(b). Note that the regions of highest numerical uncertainties correspond to the scope of highest deviation between RANS and LES as found in the previous section. Here, uncertainties in the magnitude of 300 K are present.

Following [6], the calculated numerical uncertainties of the simulated temperature profiles are treated as purely epistemic uncertainties and will be added as an interval to the results of the later propagation of input uncertainties. We will use the reference grid $f_2$ for the further sensitivity analysis and propagation of input uncertainties.

### 5.2. Reduction of input parameter space: MOAT screening

A screening of the input parameter space from Table 3 is performed using MOAT sensitivity analysis as described previously. As a result, the influence of the input parameters on the gas phase temperature can be assessed. For the MOAT screening a total number of 28 RANS simulations are run resulting in $r = 4$ elementary effects for each of the 6 input parameters. According to [61], $r = 4$ is the minimum value to place confidence in the method, while keeping the computational expense at a minimum. For the analysis of the results, the modified mean $\mu^*$ as recommended by [62] is used instead of the original $\mu$ from Eq. (4). For the computation of $\mu^*$ the absolute value of the elementary effect $d_i$ is considered to overcome the effect of alternating signs in $d_i$.

MOAT analysis is performed for the radial profiles of temperature at the six axial positions where experimental data is available ($z = \{15, 20, 30, 40, 50, 60\}$ mm). This allows for a characterization of the sensitivity with proceeding evaporation and reaction over the flame. The results are shown in the upper plot of Fig. 7. Data is plotted in a $\mu^* - \sigma$ space which enables a fast classification of sensitivities: linear or direct effects increase along the $\mu^*$ axis while non-linear or interaction effects advance along the $\sigma$ axis. Consequently, high influence parameters are found on the right and upper portion of the $\mu^* - \sigma$ space. Labels at the data points in Fig. 7 indicate its $z$ – position in the computational domain.

Highest linear and interaction effects are visible for mean trajectory angle $\bar{\varphi}$ and dispersion angle $\varphi'$ although both decrease in magnitude with increasing distance from the boundary condition. It is assumed that the strong interaction effect arises from the fact that both parameters determine the opening angle of the spray cone. As the effect of the other four parameters is

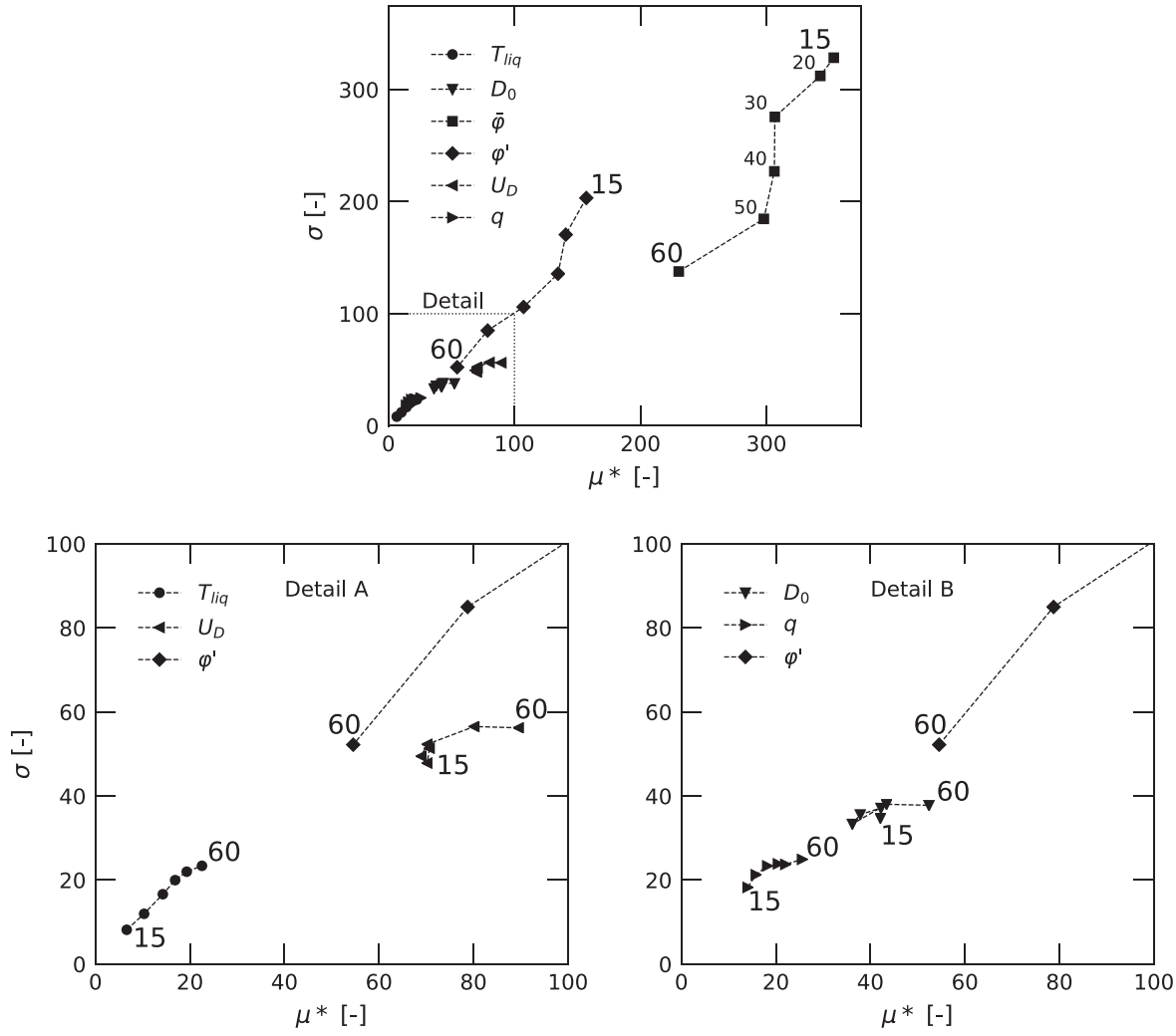


**Fig. 7.** Standard deviation $\sigma$ of elementary effects for temperature plotted against their modified mean $\mu^*$ from MOAT analysis. Labels indicate axial positions $z$.

substantially smaller, a detail of the lower left portion of the $\mu^* - \sigma$ space is included in Fig. 7. In contrast to $\bar{\varphi}$ and $\varphi'$, the relative influence of liquid droplet temperature $T_{liq}$, droplet starting velocity $U_D$, distribution factor $q$ and mean droplet diameter $D_0$ rises with increasing $z$ – position. However, in particular $T_{liq}$ and $q$ have only minor influence on the temperature when compared to $\bar{\varphi}$ and $\varphi'$. It is therefore concluded that these two parameters can be fixed to the reference values from Table 3 and neglected for the following uncertainty quantification. Thus, the uncertain input parameter space $\Omega$ is reduced to $\Omega_r$ comprising $\bar{\varphi}$, $\varphi'$, $D_0$ and $U_D$ with the respective bounds from Table 3.

### 5.3. Surrogate modeling: PCE construction and testing

For the propagation of input uncertainties a PCE approximation of the RANS simulation model is constructed over the reduced input parameter space $\Omega_r$. Sandia DAKOTA 6.4 [63] is utilized for the construction and evaluation of PCE models.

In order to apply the PCE framework to a specific problem, a structure for the multivariate polynomials $\Psi_k$ in the PCE must be specified. As $\Psi_k = f(\boldsymbol{\xi})$ this choice depends on the structure of the random input $\boldsymbol{\xi}$. An overview of suitable polynomial basis functions with corresponding probability distributions of $\boldsymbol{\xi}$ is given in the generalized Wiener–Askey scheme [64]. For the PCE construction, we define the uncertain inputs to be uniformly distributed over $\Omega_r$ and therefore apply the uniform transformation $\xi_i \sim \mathcal{U}(-1, 1)$ corresponding to Legendre polynomials for $\Psi_k$. Note that this is only valid under the assumption of uncorrelated inputs.

The main computational effort has to be put in the calculation of PCE coefficients $\alpha_k$ through the evaluation of the spectral projection from Eq. (8). We use multidimensional numerical integration based on the Smolyak sparse grid tensorization method [8] in combination with a nested Gauss–Patterson quadrature rule [65]. In the sparse grid approach, different grid levels are considered, corresponding to different orders of accuracy of the resulting PCE. A level-1 expansion (L1) of the four-dimensional input space $\Omega_r$ requires 9 quadrature points which increases to 49 points for a level-2 expansion (L2). Each quadrature point requires an evaluation of the RANS simulation model. Due to the choice of a nested quadrature rule, points of the L1 expansion are a subset of the L2 points. Note that a level-2 expansion of the original six-dimensional input space $\Omega$ would require 97 points which highlights the importance of *a priori* sensitivity analysis and reduction of stochastic dimension.

PCE accuracy is examined through holdout validation against additional RANS model evaluations independent from the quadrature points. From a previous study [66], 40 holdout datasets are available. These test points were distributed over $\Omega_r$ using a low discrepancy Sobol sequence [67] which allows for a consistent evaluation of PCE prediction quality. A qualitative comparison of radial temperature profiles from RANS simulation and PCE with different expansion order at an exemplary holdout test point is

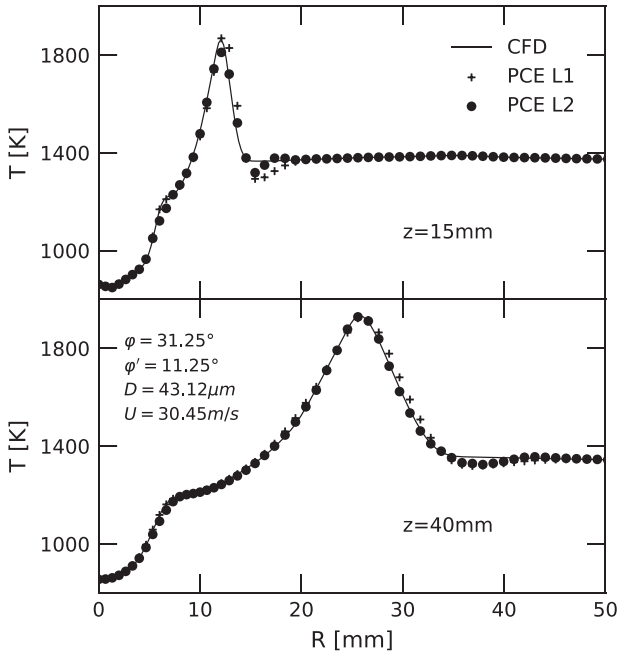


**Fig. 8.** Comparison of temperature profiles from RANS simulation and PCE prediction.

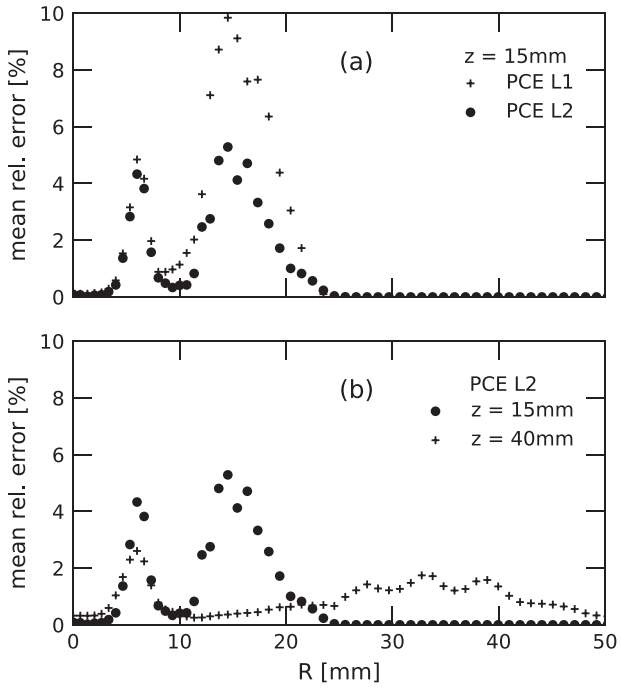


**Fig. 9.** PCE prediction error $\varepsilon_{PCE}$.

given in Fig. 8. Both expansions are able to predict the data with high accuracy at both axial positions. Minor improvements are achieved when considering an L2 expansion instead of L1. At $z = 15$ mm both expansions fail to precisely meet the transition from the flame front to the coflow ($r = 15$ mm). Note that this behavior is also found when analyzing the other holdout datasets.

A quantitative representation of PCE accuracy is calculated using the normalized root mean squared error $\varepsilon_{PCE} = ||\mathcal{M}_{\mathcal{PCE}} - \mathcal{M}||_2 / ||\mathcal{M}||_2$ which resembles the mean relative deviation between PCE and RANS over the 40 holdout datasets. Radial profiles of the error at $z = 15$ mm are displayed in the upper part of Fig. 9 for the two expansion levels. Mean error stays below 10% for the L1 case and reduces to a maximum of 6% in the L2 case. As discussed previously, maximum error is found in the flame-coflow transition region. Certainly, this region profits the most from the L2 expansion. A comparison of $\varepsilon_{PCE}$ from the L2 expansion at two different axial positions is illustrated in the lower part of Fig. 9: Prediction quality is increased at the further downstream position. This tendency is also present at the other axial positions which are not shown here for brevity.

Considering that the PCE approximation will reduce the computing time for uncertainty quantification by several orders of magnitude, the accuracy of the L2 expansion is seen as sufficient.

### 5.4. Forward propagation of input uncertainties

Uncertainties in the output quantities of interest, i.e. temperature profiles, can now be quantified via a forward propagation of the input uncertainties in $\Omega_r$ using the L2 PCE as a surrogate model. All four input parameters are treated as purely epistemic interval-valued uncertainties bounded by the minimum and maximum as summarized in Table 3. Due to the epistemic nature of the input uncertainties, the Probability Bounds Analysis framework (PBA) [6,68] is utilized. Within this framework, minimum and maximum bounds for a QoI are computed rather than precise distribution functions. This is motivated by the lack of knowledge arising from the imprecise probability distribution function in the input of the forward propagation.

**Table 4**
Sampling statistics over the reduced input space $\Omega_r$: LHS / analytical solution

| Case | $\mu$ | $\sigma$ | $\gamma$ |
|---|---|---|---|
| $D_0$ [$\mu$m] | 42.5 / 42.5 | 2.0835 / 2.0833 | $4 \cdot 10^{-6}$ / 0 |
| $U_D$ [m s$^{-1}$] | 35 / 35 | 0.1455 / 0.1455 | $3 \cdot 10^{-4}$ / 0 |
| $\bar{\varphi}$ [°] | 13 / 13 | 0.2851 / 0.2851 | $2 \cdot 10^{-5}$ / 0 |
| $\varphi'$ [°] | 31.5 / 31.5 | 5.8806 / 5.8801 | $5 \cdot 10^{-6}$ / 0 |

Bounds are obtained by Latin Hypercube Sampling (LHS) [37] of the PCE surrogate model over $\Omega_r$. A space filling, uniform sampling over $\Omega_r$ is required in PBA, since each sample from $\Omega_r$ is treated as a possible value instead of a value associated with a probability [6]. $10^4$ samples are drawn from the PCE surrogate model within a few minutes of computing time. Sampling statistics regarding mean $\mu$, variance $\sigma$ and skewness $\gamma$ of the LHS sampling are summarized in Table 4 and compared to the analytical solution of a uniform distribution. All moments are approximated with very high accuracy using $10^4$ samples. The sample size is therefore seen as sufficient.

Resulting temperature realizations and corresponding bounds are shown in Fig. 10. As a consequence of the PBA framework and the epistemic input all realizations are assigned an equal probability of unity. Therefore, the gray area represents the uncertainty region in the temperature results given the uncertainties in the input. In addition, the deterministic reference simulation from Section 5.1 is indicated by dashed lines. Highest uncertainties exist around the region of peak temperature at all axial positions indicating that the spray input parameters significantly influence the position of the flame. Over all radial positions in the flame region an uncertainty level between 100K and 1400K is found.

Regions exist where the UQ based simulation is unable to bracket the experimental data, especially at $5 < R < 10$ mm for $z = 15$ and 20 mm. Reason for this could be further uncertainties which are not included in the analysis, a general modeling error of the used simulation model or uncertainties and measurement errors in the experimental data which are probably larger than reported. Since a major deviation between RANS and LES and high

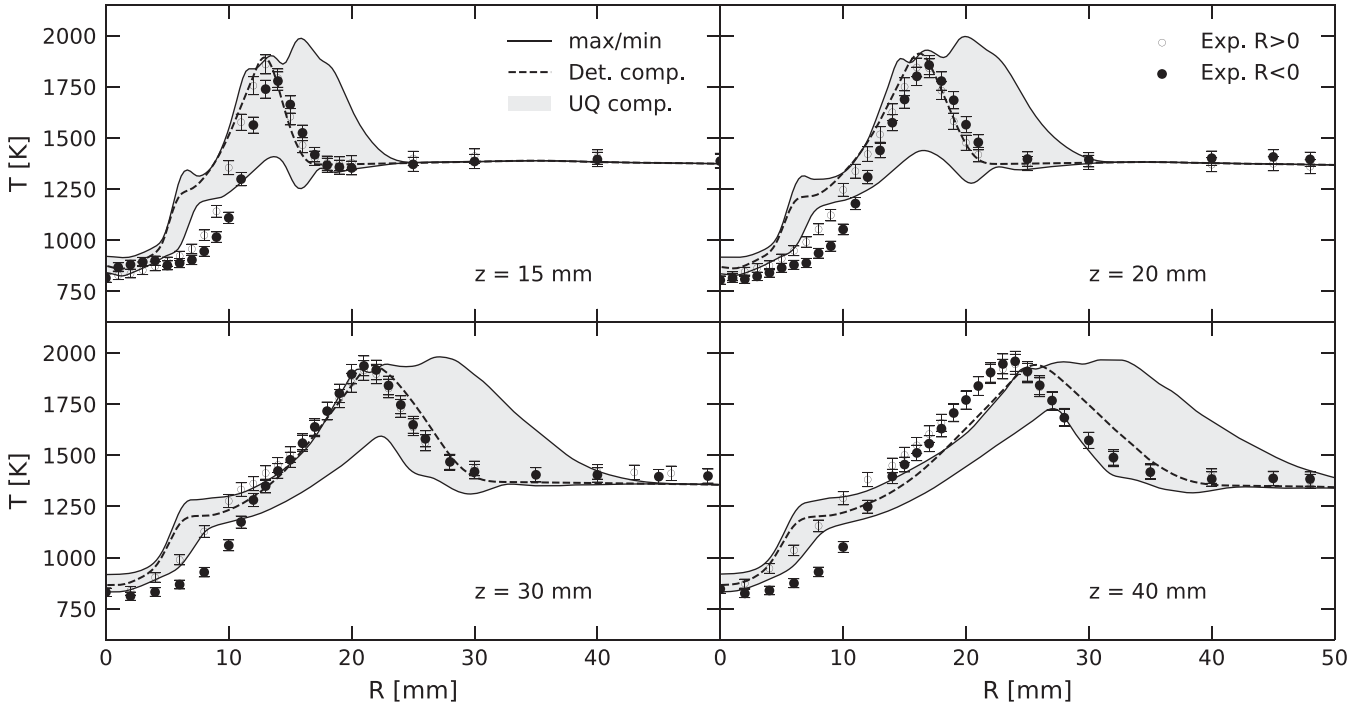


**Fig. 10.** PCE based uncertainty regions for DSHC $\mathbf{H_{II}}$ case.

**Table 5**
Computing time statistics for the used UQ methods.

| Case | Runs | CPU hours [h] |
|---|---|---|
| L2 PCE of $\Omega$ | 97 | 32600 |
| L2 PCE of $\Omega_r$ | 49 | 16500 |
| MOAT of $\Omega$ | 28 | 9500 |

numerical uncertainties in this region were found in the previous sections, it is most likely that a modeling error in the RANS is propagated through the PCE surrogate model. In contrast, the bias in experimental data for $R < 10$ mm at $z = 30$ and 40 mm prohibits a definitive evaluation of simulation credibility at this position as experimental data for $R > 0$ mm is within the uncertainty region but not the portion from $R < 0$ mm.

Oscillating bounds around the peak temperature at $z = 15$ and 20 mm coincide with high PCE prediction errors as evident from Fig. 9. Hence, they are assumed to be a result of outliners in the uncertainty propagation.

#### 5.4.1. Effects of parameter reduction

In order to assess the influence of parameter space reduction on the PBA results, an L2 PCE expansion of the original parameter space $\Omega$ is calculated and used for forward propagation, too. Resulting bounds are compared to the outcome of the reduced parameter space $\Omega_r$ in Fig. 11. No significant deviations between the two bounded areas are observable, confirming that the parameter reduction does not affect the results of the PBA in the case considered. As already suspected in the MOAT analysis, the four parameters in $\Omega_r$ essentially contribute to the variance in the temperature profiles.

Computing time statistics for the different methods in the UQ process are summarized in Table 5. L2 PCE of $\Omega$ corresponds to the aforementioned sampling of the full parameter space. Based on the statistics it is deduced that the proposed workflow of parameter space reduction (MOAT) and sampling of the reduced parameter space $\Omega_r$ already results in a 20% reduction in computing time, although the parameter space is only slightly reduced from six to four parameters. Note that this reduction increases in cases with further parameter reduction.

In the following, results from the PBA over $\Omega_r$ are again used for further analysis.

### 5.5. A posteriori sensitivity analysis

To appraise the contribution of the uncertain input parameters to the high variance in the simulation results indicated by the uncertainty region, first order and total order Sobol' indices are derived from the PC expansion following Eq. (5). For a simplified interpretation, indices are aggregated over the radial coordinate by weighting the local index $S(r)$ with the local variance in PCE temperature predictions [69]:

$$\boldsymbol{S} = \frac{\int_R \mathbb{V}[\mathcal{M}_{PCE}(r)]S(r)\mathrm{d}r}{\int_R \mathbb{V}[\mathcal{M}_{PCE}(r)]\mathrm{d}r} \tag{16}$$

Aggregated Sobol' indices $\boldsymbol{S}$ for temperature at different axial positions are given in Fig. 12. Solid bars illustrate first order indices $\boldsymbol{S}$, i.e. the direct contribution of a parameter to the variance, whereas augmented hatched bars indicate total indices $\boldsymbol{S_T}$ which include interactions with other parameters. As a result, it follows that $\boldsymbol{S_T} \geq \boldsymbol{S}$. Mean injection angle $\bar{\varphi}$ is identified as the dominant parameter over all axial positions, causing more than 60° of variance in temperature. Close to the injector, $U_D$ demonstrates some influence, yet with decreasing magnitude. The minor influence of $\varphi'$ rises with increasing $z$ position. It should be pointed out that differences between $\boldsymbol{S}$ and $\boldsymbol{S^T}$ are only observable for $\bar{\varphi}$ and $U_D$, which indicates a coupled effect between the two parameters.

To clarify the influence of $\boldsymbol{\varphi}$, profiles of local Sobol' indices $S(r)$ are shown in Fig. 13 for $z = 40$ mm. Highest $S$ for $\boldsymbol{\varphi}$ are present at the outer flame region ($R > 25$ mm). Here, influence of other parameters are negligible. As $\bar{\varphi}$ corresponds to the spray cone opening angle, $\bar{\varphi}$ primarily determines the radial position of liquid droplets. In the outer flame region, this is closely connected to

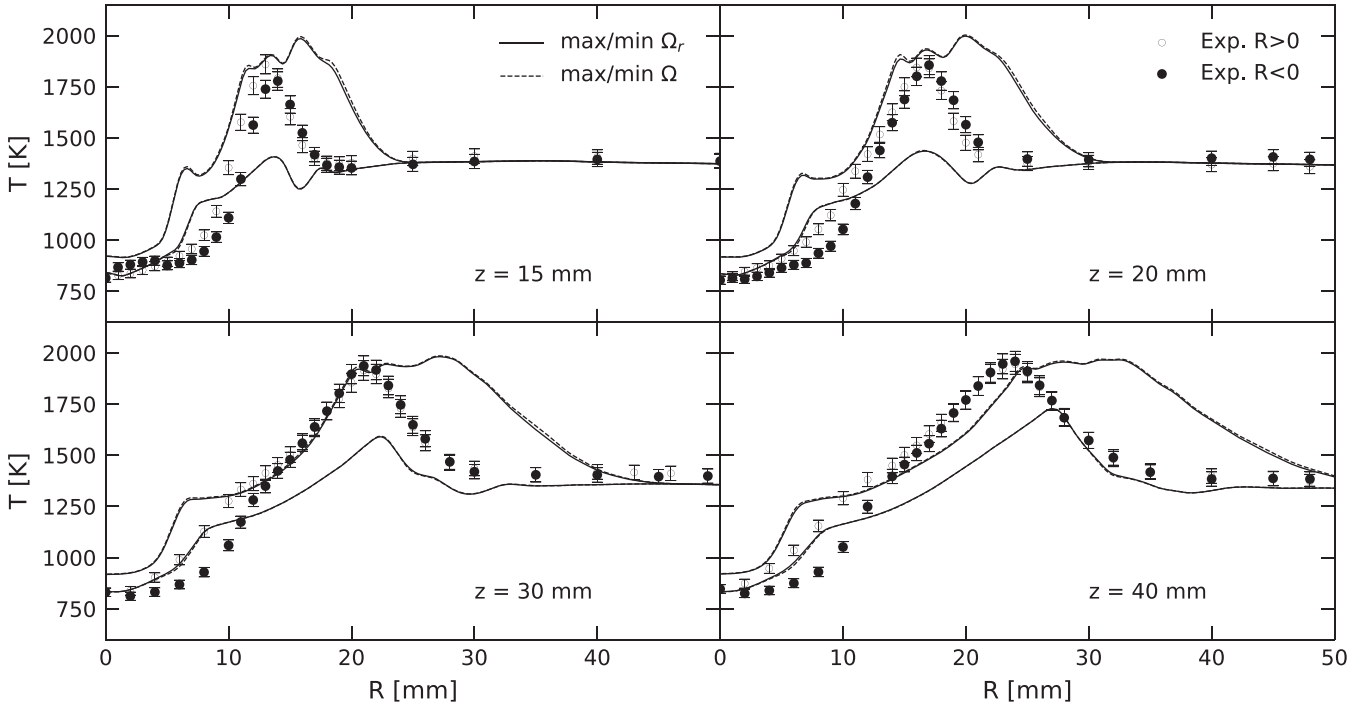


**Fig. 11.** Probability bounds of computed temperature profiles for the full ($\Omega$) and reduced ($\Omega_r$) input parameter space.

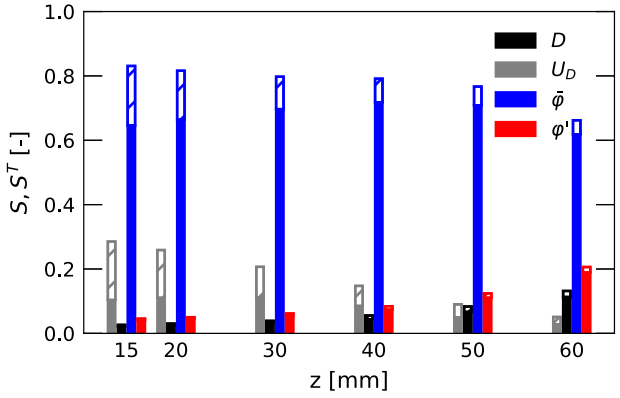


**Fig. 12.** Aggregated Sobol' indices for temperature. Hatched bars indicate total indices.

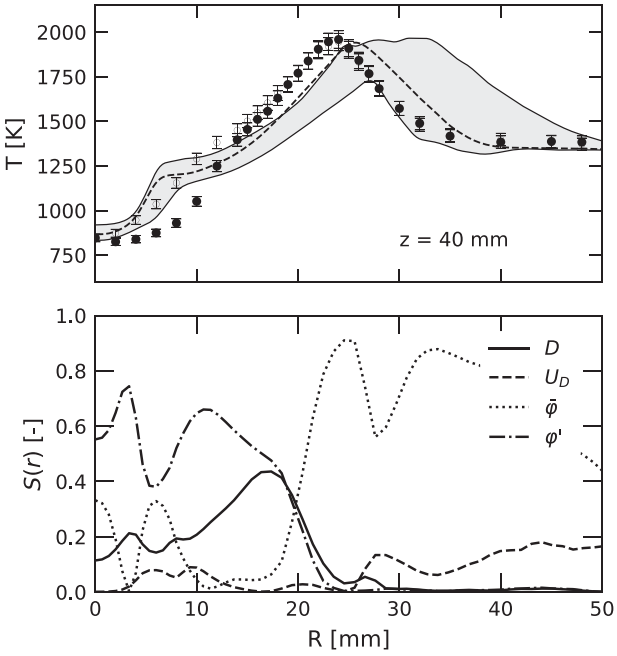


**Fig. 13.** Local Sobol' indices for temperature at z=40 mm.

the supply of gaseous ethanol to the reaction zone. Consequently, changes in $\bar{\varphi}$ shift and stretch the temperature profile along $R$ and cause high uncertainties in the outer flame region. In contrast, influence of $\bar{\varphi}$ drops in the inner flame region and the droplet diameter $D$ becomes more dominant. This reaction zone is formed by the fuel rich premixed reaction of ethanol vapor as a result of strong evaporation of droplets [56]. As $D$ is the only uncertain parameter directly connected to evaporation, it influences the evaporation process in this region and contributes to the variance in temperature.

Note that the discussed phenomena are also found at the other axial positions.

### 5.6. Determination of total uncertainty

Finally, total uncertainty in the considered simulation is determined using the method of composite probability boxes ($p$-boxes) [7]. Due to the functional nature of the output QoI, this is only illustrated exemplarily at three distinct points in the simulation domain. Results are presented in Fig. 14. A $p$-box consists of the cumulative distribution function (CDF) of the QoI which was obtained by propagating the input uncertainty with the help of the PCE surrogate model. Furthermore, numerical uncertainties $U_{num.}$ and PCE prediction errors $U_{PCE}$ from Sections 5.1 and 5.3 are appended to both sides of the CDF. This is motivated by the epistemic nature of these uncertainties [6]. Again, the CDF from input uncertainties is given as brackets without a probability structure inside the $p$-box as a result of the interval-valued input. Owing to the deterministic approach, results from the reference simulation are shown as Dirac pulses (dashed vertical lines).

At all three positions total predictive uncertainty is primarily due to the uncertainties in the model inputs. Additional PCE uncertainty is visible at the first two positions, while numerical

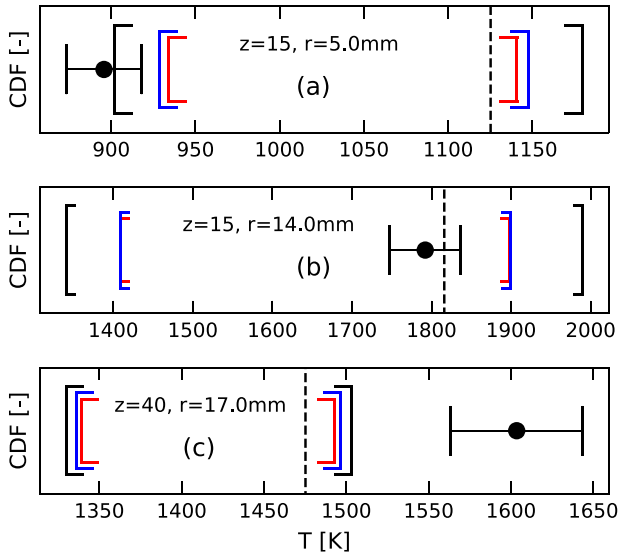


**Fig. 14.** Probability box for temperature: (—) $U_{in}$, (—) $U_{in}+U_{num}$, (—) $U_{in}+U_{num}+U_{PCE}$, (– –) det. ref. simulation, (•) exp. $R>0$ mm.

uncertainties are negligible compared to the magnitude of $U_{in}$. Even when considering all three types of uncertainties, experimental data at $z=40$, $R=17$ mm (Fig. 14(c)) cannot be met by the simulation which further affirms the presence of a general modeling error. While the calibrated deterministic simulation precisely meets the experiment in Fig. 14(b), the uncertainty quantification reveals notable uncertainties of 500 K at this position.

## 6. Summary and conclusions

The present study successfully demonstrated the use of non-intrusive Polynomial Chaos Expansion for forward uncertainty quantification and sensitivity analysis in the simulation of turbulent spray combustion. Profiles of temperature over the reaction zone in a laboratory scale spray flame were considered as output quantities of interest. Since major input uncertainties arise from the parameters of the spray boundary condition, they were treated as epistemic uncertainties with the respective bounds derived from an analysis of existing simulations in literature. Uncertainties in the used RANS simulation model and the PCE surrogate model were evaluated by means of solution extrapolation and holdout validation, respectively. Based on the findings of an *a priori* MOAT sensitivity analysis, the stochastic dimension of the input was reduced to the four most influential parameters. The computational inexpensive PCE surrogate models were explored using Latin Hypercube Sampling to obtain probabilistic bounds of the QoI under the given uncertainties. Thus, an extensive uncertainty region around the deterministic reference simulation was revealed. Regions were identified where the UQ based simulation is unable to bracket the experimental data. This was attributed to a general modeling error. From an *a posteriori* sensitivity analysis, the majority of variance in the QoI was connected to the spray cone angle of the atomizer which controls the position of the droplets and transport of gaseous fuel to the reaction zone.

On the basis of these findings we draw the following conclusions:

- PCE enables non-intrusive probabilistic methods for complex applications with minor loss in accuracy compared to the high fidelity simulation model.
- The comparison of all sources of uncertainties confirmed that the total predictive uncertainty in the case considered is primarily due to the input uncertainties.
- Systematic uncertainty quantification requires identification and adequate characterization of all sources of uncertainties. Therefore, a precise definition of input uncertainties by means of PDFs should be included in the design of validation experiments.
- UQ studies can provide guidelines for the improvement of experiments. In the case presented, a precise experimental measurement of the spray mean trajectory angle $\bar{\varphi}$ would significantly decrease the uncertainties in the simulation.

As the goal of this study was to demonstrate the ability and applicability of available UQ tools to spray combustion simulation, not all effects in the QoI were described and discussed. A thorough physical interpretation including additional QoIs (gas field velocity, evaporated mass fraction) will be subject to future work. Furthermore, one has to keep in mind that results from a UQ study must always be interpreted with respect to the assumption on bounds and distributions made for the uncertain input space. In the present work, these were derived taking into account the findings of existing simulations in literature. Other approaches could include reported uncertainties from experiments or expert knowledge based on experience and empirical data.

Finally, it should be pointed out that model form uncertainties were not considered. However, as spray combustion simulation involves a variety of strongly coupled models, model form uncertainties could be a significant contributor to the total uncertainty in the QoI [7] and should be therefore included in a future study.

It was shown that UQ methods help to understand sensitivities of simulation results and provide a more reliable basis for validation against experimental data and evaluation of simulation credibility. In the engineering application these methods present quantitative information about the confidence in the predicted performance from a simulation model. On that basis, risk informed decision making is facilitated to safely meet performance targets such as emissions or efficiency.

## Declaration of Competing Interest

The authors whose names are listed immediately below certify that they have NO affi liations with or involvement in any organization or entity with any fi nancial interest (such as honoraria; educational grants; participation in speakersbureaus; membership, employment, consultancies, stock ownership, or other equity interest; and expert testimony or patent-licensing arrangements), or non-financial interest (such as personal or professional relationships, affiliations, knowledge or beliefs) in the subject matter or materials discussed in this manuscript.

The authors whose names are listed immediately below report the following details of affiliation or involvement in an organization or entity with a financial or non-financial interest in the subject matter or materials discussed in this manuscript. Please specify the nature of the conflict on a separate sheet of paper if the space below is inadequate.

## Acknowledgments

The authors would like to thank Prof. D. M. Roekarts from TU Delft for providing the experimental database on the DSHC flame.

## References

[1] L.Y. Gicquel, G. Staffelbach, T. Poinsot, Large eddy simulations of gaseous flames in gas turbine combustion chambers, Prog. Energ. Combust. 38 (6) (2012) 782–817.
[2] S. Hochgreb, Mind the gap: Turbulent combustion model validation and future needs, Proc. Combust. Inst. 37 (2) (2019) 2091–2107.
[3] V. Raman, M. Hassanaly, Emerging trends in numerical simulations of combustion systems, Proc. Combust. Inst. 37 (2) (2019) 2073–2089.

[4] A. Masri, Turbulent combustion of sprays: From dilute to dense, Combust. Sci. Technol. 188 (10) (2016) 1619–1639.
[5] P.J. Roache, Fundamentals of verification and validation, Hermosa Publishers, 2009.
[6] W.L. Oberkampf, C.J. Roy, Verification and validation in scientific computing, Cambridge University Press, 2010.
[7] C.J. Roy, W.L. Oberkampf, A comprehensive framework for verification, validation, and uncertainty quantification in scientific computing, Comput. Method Appl. M. 200 (25) (2011) 2131–2144.
[8] O. Le Maître, O.M. Knio, Spectral methods for uncertainty quantification: with applications to computational fluid dynamics, Springer Science & Business Media, 2010.
[9] K. Sepahvand, S. Marburg, H.-J. Hardtke, Uncertainty quantification in stochastic systems using polynomial chaos expansion, Int. J. Appl. Mech. 2 (02) (2010) 305–353.
[10] M.V.C. de Souza, M.J. Colaço, A.J.K. Leiroz, Application of the generalized polynomial chaos expansion to the simulation of an internal combustion engine with uncertainties, Fuel 134 (2014) 358–367.
[11] J. Prager, H.N. Najm, K. Sargsyan, C. Safta, W.J. Pitz, Uncertainty quantification of reaction mechanisms accounting for correlations introduced by rate rules and fitted Arrhenius parameters, Combust. Flame 160 (9) (2013) 1583–1593.
[12] M.E. Mueller, V. Raman, Model form uncertainty quantification in turbulent combustion simulations: Peer models, Combust. Flame 187 (2018) 137–146.
[13] R. Johnson, H. Wu, M. Ihme, A general probabilistic approach for the quantitative assessment of LES combustion models, Combust. Flame 183 (2017) 88–101.
[14] A. Avdonin, S. Jaensch, C.F. Silva, M. Češnovar, W. Polifke, Uncertainty quantification and sensitivity analysis of thermoacoustic stability with non-intrusive polynomial chaos expansion, Combust. Flame 189 (2018) 300–310.
[15] B. Rauch, P. Le Clercq, M. Aigner, Application of uncertainty quantification for the validation of spray evaporation models, ILASS â Europe 2016, 27th Annual Conference on Liquid Atomization and Spray Systems (2016).
[16] N. Van Dam, C. Rutland, Uncertainty quantification of large-eddy spray simulations, J. Verif. Valid. Uncertain. Quant. 1 (2) (2016) 021006.
[17] M.E. Mueller, G. Iaccarino, H. Pitsch, Chemical kinetic uncertainty quantification for Large Eddy Simulation of turbulent nonpremixed combustion, P. Combust. Inst. 34 (1) (2013) 1299–1306.
[18] Y. Pei, M.J. Davis, L.M. Pickett, S. Som, Engine combustion network (ECN): Global sensitivity analysis of spray a for different combustion vessels, Combust. Flame 162 (6) (2015) 2337–2347.
[19] M.E. Mueller, V. Raman, Effects of turbulent combustion modeling errors on soot evolution in a turbulent nonpremixed jet flame, Combust. Flame 161 (7) (2014) 1842–1848.
[20] Y. Tang, M. Hassanaly, V. Raman, B. Sforzo, J. Seitzman, A comprehensive modeling procedure for estimating statistical properties of forced ignition, Combust. Flame 206 (2019) 158–176.
[21] M. Khalil, G. Lacaze, J.C. Oefelein, H.N. Najm, Uncertainty quantification in LES of a turbulent bluff-body stabilized flame, Proc. Combust. Inst. 35 (2) (2015) 1147–1156.
[22] M. Masquelet, J. Yan, A. Dord, G. Laskowski, L. Shunn, L. Jofre, G. Iaccarino, Uncertainty quantification in large eddy simulations of a rich-dome aviation gas turbine, ASME Turbo Expo (2017). GT2017-64835
[23] W. Jones, A. Marquis, K. Vogiatzaki, Large-eddy simulation of spray combustion in a gas turbine combustor, Combust. Flame 161 (1) (2014) 222–239.
[24] B. Enderle, F. Grimm, G. Eckel, M. Aigner, Large eddy simulation of turbulent ethanol spray flames under MILD conditions using a finite rate chemistry combustion model, ICLASS 2018, 14th Triennial International Conference on Liquid Atomization and Spray Systems (2018).
[25] M.D. Domenico, Numerical simulations of soot formation in turbulent flows, University of Stuttgart, 2008 Ph.D. thesis.
[26] M. Di Domenico, P. Gerlinger, B. Noll, Numerical simulations of confined, turbulent, lean, premixed flames using a detailed chemistry combustion model, ASME Turbo Expo (2011). GT2011-45520
[27] W. Jones, B.E. Launder, The prediction of laminarization with a two-equation model of turbulence, Int. J. Heat Mass Transf. 15 (2) (1972) 301–314.
[28] P. Gerlinger, Numerische Verbrennungssimulation: Effiziente numerische Simulation turbulenter Verbrennung, Springer-Verlag, 2005.
[29] O. Röhl, N. Peters, A reduced mechanism for ethanol oxidation, 4th European Combustion Meeting (ECM 2009), Vienna, Austria, April (2009), pp. 14–17.
[30] G. Eckel, J. Grohmann, L. Cantu, N. Slavinskaya, T. Kathrotia, M. Rachner, P. Le Clercq, W. Meier, M. Aigner, LES of a swirl-stabilized kerosene spray flame with a multi-component vaporization model and detailed chemistry, Combust. Flame 207 (2019) 134–152.
[31] P. Jenny, D. Roekaerts, N. Beishuizen, Modeling of turbulent dilute spray combustion, Prog. Energy Combust. 38 (6) (2012) 846–887.
[32] B. Abramzon, W. Sirignano, Droplet vaporization model for spray combustion calculations, Int. J. Heat Mass Transf. 32 (9) (1989) 1605–1618.
[33] F.X. Tanner, A cascade atomization and drop breakup model for the simulation of high-pressure liquid jets, Technical Report, SAE Technical Paper, 2003.
[34] A. Gosman, E. Loannides, Aspects of computer simulation of liquid-fueled combustors, J. Energy 7 (6) (1983) 482–490.
[35] G. Eckel, Large Eddy Simulation of Turbulent Reacting Multi-Phase Flows, University of Stuttgart, 2018 Ph.D. thesis.
[36] G. Eckel, P. Le Clercq, T. Kathrotia, A. Saenger, S. Fleck, M. Mancini, T. Kolb, M. Aigner, Entrained flow gasification. Part 3: Insight into the injector near–field by large eddy simulation with detailed chemistry, Fuel 223 (2018) 164–178.
[37] G. Fishman, Monte Carlo: concepts, algorithms, and applications, Springer Science & Business Media, 2013.
[38] A. Forrester, A. Keane, et al., Engineering design via surrogate modelling: A practical guide, John Wiley & Sons, 2008.
[39] A. Saltelli, M. Ratto, T. Andres, F. Campolongo, J. Cariboni, D. Gatelli, M. Saisana, S. Tarantola, Global sensitivity analysis: The primer, John Wiley & Sons, 2008.
[40] M.D. Morris, Factorial sampling plans for preliminary computational experiments, Technometrics 33 (2) (1991) 161–174.
[41] I.M. Sobol, Sensitivity estimates for nonlinear mathematical models, Math. Model. Comput. Exp. 1 (4) (1993) 407–414.
[42] T. Homma, A. Saltelli, Importance measures in global sensitivity analysis of nonlinear models, Reliab. Eng. Syst. Safe. 52 (1) (1996) 1–17.
[43] R.G. Ghanem, P.D. Spanos, Stochastic finite element method: Response statistics, Stochastic Finite Elements: A Spectral Approach, Springer (1991), pp. 101–119.
[44] H.N. Najm, Uncertainty quantification and polynomial chaos techniques in computational fluid dynamics, Ann. rev. fluid mech. 41 (2009) 35–52.
[45] B. Sudret, Global sensitivity analysis using polynomial chaos expansions, Reliab. Eng. Syst. Saf. 93 (7) (2008) 964–979.
[46] H.C. Rodrigues, M.J. Tummers, E.H. van Veen, D.J. Roekaerts, Spray flame structure in conventional and hot-diluted combustion regime, Combust. Flame 162 (3) (2015) 759–773.
[47] D.P. Schmidt, I. Nouar, P. Senecal, C. Rutland, J. Martin, R.D. Reitz, J.A. Hoffman, Pressure-swirl atomization in the near field, Technical Report, SAE Technical Paper, 1999.
[48] R.D. Reitz, A photographic study of flash-boiling atomization, Aerosol Sci. Tech. 12 (3) (1990) 561–569.
[49] H. Correia Rodrigues, Spray combustion in moderate and intense low-oxygen conditions: An experimental study, Delft University of Technology, 2015 Ph.D. thesis.
[50] L. Ma, D. Roekaerts, Modeling of spray jet flame under MILD condition with non-adiabatic FGM and a new conditional droplet injection model, Combust. Flame 165 (2016) 402–423.
[51] L. Ma, S. Zhu, M. Tummers, T. Van Der Meer, D. Roekaerts, Numerical investigation of ethanol spray-in-hot-coflow flame using steady flamelet model, Eighth Mediterranean Combustion Symposium (2013), pp. 1–12.
[52] S.H. Jamali, Computational Modeling of Turbulent Ethanol Spray Flames in a Hot Diluted Coflow, Delft University of Technology, 2014 Ph.D. thesis.
[53] S. Gallot-Lavallée, W. Jones, A. Marquis, Large eddy simulation of an ethanol spray flame under MILD combustion with the stochastic fields method, Proc. Combust. Inst. 36 (2) (2017) 2577–2584.
[54] L.M. Cantu, J. Grohmann, W. Meier, M. Aigner, Temperature measurements in confined swirling spray flames by vibrational coherent anti-stokes raman spectroscopy, Exp. Therm. Fluid Sci. 95 (2018) 52–59.
[55] E.H. Van Veen, D. Roekaerts, On the accuracy of temperature measurements in turbulent jet diffusion flames by coherent anti-stokes-raman spectroscopy, Combust. Sci. Technol. 175 (10) (2003) 1893–1914.
[56] L. Ma, D. Roekaerts, Numerical study of the multi-flame structure in spray combustion, Proc. Combust. Inst. 36 (2) (2017) 2603–2613.
[57] L. Ma, D. Roekaerts, Structure of spray in hot-diluted coflow flames under different coflow conditions: A numerical study, Combust. Flame 172 (2016) 20–37.
[58] N. Abani, A.F. Ghoniem, Large eddy simulations of coal gasification in an entrained flow gasifier, Fuel 104 (2013) 664–680.
[59] F. Stern, R.V. Wilson, H.W. Coleman, E.G. Paterson, Comprehensive approach to verification and validation of CFD simulationsâPart 1: Methodology and procedures, J. Fluid. Eng.-T. ASME 123 (4) (2001) 793–802.
[60] T.S. Phillips, C.J. Roy, Richardson extrapolation-based discretization uncertainty estimation for computational fluid dynamics, J. Fluid. Eng.-T. ASME 136 (12) (2014) 121401.
[61] A. Saltelli, S. Tarantola, F. Campolongo, M. Ratto, Sensitivity analysis in practice: A guide to assessing scientific models, John Wiley & Sons, 2004.
[62] F. Campolongo, J. Cariboni, A. Saltelli, An effective screening design for sensitivity analysis of large models, Environ. Modell. Softw. 22 (10) (2007) 1509–1518.
[63] B. Adams, L. Bauman, W. Bohnhoff, K. Dalbey, M. Ebeida, J. Eddy, M. Eldred, P. Hough, K. Hu, J. Jakeman, J. Stephens, L. Swiler, D. Vigil, T. Wildey, Dakota, a multilevel parallel object-oriented framework for design optimization, parameter estimation, uncertainty quantification, and sensitivity analysis: Version 6.4 userâs manual, Sandia Technical Report SAND2014-4633 (2016).
[64] D. Xiu, G.E. Karniadakis, The wiener–askey polynomial chaos for stochastic differential equations, SIAM J. Sci. Comput. 24 (2) (2002) 619–644.
[65] P.J. Davis, P. Rabinowitz, Methods of numerical integration, Courier Corporation, 2007.
[66] B. Enderle, B. Rauch, F. Grimm, M. Aigner, Towards affordable uncertainty quantification in the simulation of turbulent spray combustion via surrogate modeling, AIAA Scitech 2019 Forum (No. 2019-1727).
[67] I.M. Sobol, D. Asotsky, A. Kreinin, S. Kucherenko, Construction and comparison of high-dimensional sobol'generators, Wilmott 2011 (56) (2011) 64–79.
[68] S. Ferson, L.R. Ginzburg, Different methods are needed to propagate ignorance and variability, Reliab. Eng. Syst. Saf. 54 (2–3) (1996) 133–144.
[69] A. Marrel, N. Saint-Geours, M. De Lozzo, Sensitivity analysis of spatial and/or temporal phenomena, Handbook of Uncertainty Quantification, 2016, pp. 1–31. https://link.springer.com/referencework/10.1007%2F978-3-319-11259-6#about.